

Available online at [www.sciencedirect.com](http://www.sciencedirect.com)**ScienceDirect**

Physics Procedia 66 (2015) 622 – 631

Physics

**Procedia**

23rd Conference on Application of Accelerators in Research and Industry, CAARI 2014

## Undergraduate Education with the Rutgers 12-Inch Cyclotron

Timothy W. Koeth\*

*University of Maryland, IREAP, Energy Research Facility, Building 223, Paint Branch Drive, College Park, Maryland 20742, USA*

---

### Abstract

The Rutgers 12-Inch Cyclotron is a research grade accelerator dedicated to undergraduate education. From its inception, it has been intended for instruction and has been designed to demonstrate classic beam physics phenomena and provides students hands on experience with accelerator technology. The cyclotron is easily reconfigured, allowing experiments to be designed and performed within one academic semester. Our cyclotron offers students the opportunity to operate an accelerator and directly observe many fundamental beam physics concepts, including axial and radial betatron motion, destructive resonances, weak and azimuthally varying field (AVF) focusing schemes, RF and DEE voltage effects, diagnostic techniques, and perform low energy nuclear reactions. This paper emphasizes the unique beam physics measurements and beam manipulations capable at the Rutgers 12-Inch Cyclotron.

© 2015 The Authors. Published by Elsevier B.V. This is an open access article under the CC BY-NC-ND license (<http://creativecommons.org/licenses/by-nc-nd/4.0/>).

Selection and peer-review under responsibility of the Organizing Committee of CAARI 2014

*Keywords:* cyclotron; education; accelerator physics; betatron motion

---

### 1. Introduction

The Rutgers' 12-inch Cyclotron, shown in figure 1a, is located in an instructional laboratory of the Department of Physics and Astronomy at Rutgers University [1]. There, it is the centerpiece of undergraduate instruction in accelerator physics. The Rutgers' undergraduate physics curriculum requires two semesters of a Modern (Senior) Physics Lab class, and since 2001, one to three exceptional students are chosen from the fall semester's participants for a special project that this author directly mentors during the spring semester. These students are assigned a

\* Corresponding author. Tel.: 1-301-405-4952; fax: +1-301-405-6327.

*E-mail address:* [koeth@umd.edu](mailto:koeth@umd.edu)

single, semester long project with the cyclotron that provides them a real life research experience in a modern physics context. Each set of new students builds upon the previous students' work, leading to the present sophisticated machine. The evolution of our cyclotron has enjoyed the dedicated efforts of nearly two dozen students: Horvath ('01) performed initial orbit calculations; Chun and MacLynne ('02) designed and oversaw the machining of the first set of weak focusing pole tips; McCain and Friedman ('03) installed and measured the new poles; Cahl and Shelly ('04) constructed a 2-D field mapper, Barker ('05) designed an auto-tuner for the high power radio frequency (RF) system; Ponter ('09) designed and commissioned an electrostatic beam deflection channel; Ruisard, Hine, and Rosenberg ('10) designed and constructed a set of spiral sector azimuthally varying field pole tips; Atay ('12) simulated the cyclotron's central region; Burcher, Gonski, and Lazarov ('13) experimentally measured the beam bunch length within one RF cycle; and most recently Reingold, Leipold, and Moreno developed fluorine based internal targets, a magnetic field insensitive high energy gamma ray detector, and attempted the  $^{19}\text{F}(p,\alpha\gamma)^{16}\text{O}$  low energy nuclear reaction [2]. As will be discussed later, this cyclotron experience has been pivotal in influencing more than one quarter of our students' subsequent career paths. While the Rutgers Cyclotron program provides a wide breadth of experiments and demonstrations, this paper will concentrate on the cyclotron's most unique educational offering: beam dynamics.

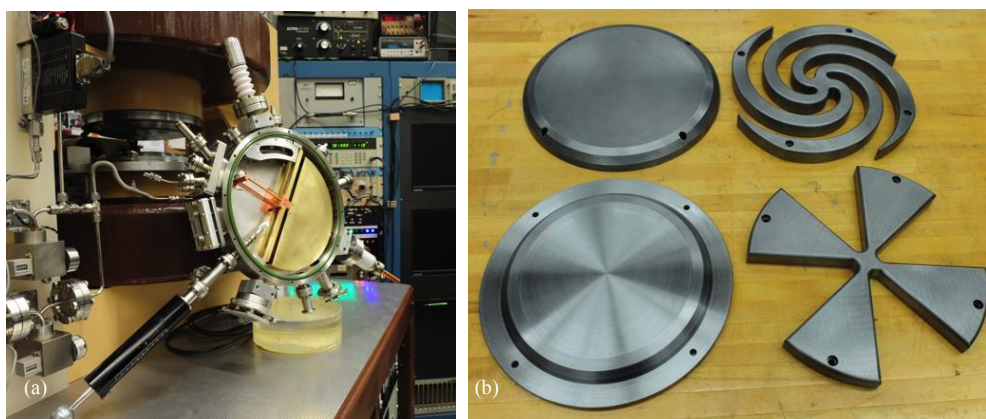


Fig. 1. (a) Rutgers 12-Inch Cyclotron chamber removed and open; (b) Repertoire of pole tips.

### 1.1. Cyclotron Description

The cyclotron magnet is an iron dominated rectangular H-frame magnet with 12 inch diameter poles pieces forming a 4-inch gap to which upper and lower pole tips up to 1-inch thick can be easily attached and removed – we currently have four sets of pole tips and one of each set is shown in figure 1b. They consist of two weak focusing (one “good” and one intentionally “bad” for educational purposes), a radial sector azimuthally varying field (AVF) and a spiral sector AVF, all capable of producing a maximum central axial field,  $B_z(r=0)$ , of 1.2 Tesla [3,4]. The magnet's upper and lower coils are independently energized enabling an intentional axial field imbalance so as to vertically shift the accelerating plane. The cyclotron has a single 5-inch radius DEE with a 0.9 inch vertical aperture and a matching dummy DEE. The Radio Frequency (RF) supply is tunable from 2 to 30 MHz with adjustable power up to 1.5 kW; it can be operated in a continuous or pulsed mode and is capable of achieving a peak DEE voltages on the order of 10 kV [5]. The ion source is an internal cold cathode Penning Ion Gauge (PIG) source that operates in excess of 40 hours before requiring service [6]. Beam diagnostics include a radial probe carrying an electrically isolated phosphor plate, which provides transverse beam images as well as beam current measurements at all radii. A demountable electrostatic deflection channel intercepts the ion beam at the 4-inch radius and is used as a velocity filter to measure ion energy [7]. A mechanically backed 4-inch diffusion pump stack supplemented with liquid nitrogen cooled baffles provides the 2-inch tall, 13-inch diameter cyclotron vacuum chamber's operating pressure of  $1\text{E}-5$  Torr. The cyclotron chamber rests on three leveling pillars for vertical alignment and the

chamber's horizontal position can be moved with respect to the magnet's center so as to introduce intentional positioning errors.

A full 3D Simion model has been developed and extensively verified with every configuration of our cyclotron [8]. This code is also used to design experimental poletips, characterize limits of beam stability, and interpret experimental measurements. Utilized in parallel with theory and experiment, the Simion simulations complete the accelerator physics' students education.

## 2. Beam Physics Demonstration

### 2.1. Orbit Stability with Weak Focusing

Weak focusing (WF), empirically discovered in the first cyclotrons, and subsequently studied by Wilson, is an ideal introduction into beam orbit stability [9]. WF fields are, at some level, present in all cyclotrons - especially in the central region. The weak focusing field is deliberately generated by slightly tapering the pole tips with azimuthal symmetry. Envisioning the field lines in the magnet gap, as viewed from the side, the reader sees a slight radial bulging of the field lines.  $\nabla \times B = 0$  states that the bulging will cause a radial magnetic field component, to first order, that grows linearly in strength with displacement above and below the accelerating (median) plane. The accelerating plane is therefore symmetrically located between the upper and lower magnetic field volumes which contain a non-zero radial component; by definition, the magnetic field is strictly vertical in the median plane. Circulating ions wandering above or below the median plane will experience an axial force,  $F_z = qv_\theta B_r$ , which, if chosen properly returns them toward the median plane.

As a consequence of the pole tip tapering, weak focusing employs an axial magnetic field,  $B_z(r)$ , that must continuously change with increasing radius,  $r$ . A field index,  $n$ , is defined as:

$$n = -\frac{r}{B} \frac{dB}{dr},$$

with three possible cases for  $n$ ;  $n < 0$ :  $B_z$  increases with  $r$ ,  $n=0$ :  $B_z$  is uniform, and  $n > 0$ :  $B_z$  decreases with  $r$ . It can be shown that for positive  $n$ , hence a decreasing  $B_z(r)$ , ions axially oscillate about the median plane with a frequency  $f_z$ :

$$f_z = \sqrt{n} f_o$$

Where  $f_o$  is the orbit revolution [cyclotron] frequency. We then define the axial "tune" as  $\nu_z$ :

$$\nu_z = \frac{f_z}{f_o} = \sqrt{n}$$

Similarly, the radial "tune" can be shown to be:

$$\nu_x = \frac{f_x}{f_o} = \sqrt{1-n}$$

It follows that for axial stability,  $n$  must be greater than 0, and for radial stability  $n$  must be less than 1. Total transverse stability exists in the region of:

$$0 < n < 1$$

Coupling resonances between the transverse motions further limit the value of  $n$ . Values of  $n=0.2, 0.25, 0.33, 0.5$  (and others yet higher) need to be avoided. Since the ions begin their spiral journey at  $r=0$  necessarily  $n$  also starts at 0, and will only climb as the radius increases; if  $n=0.2$  is to be avoided ( $\nu_x=2\nu_z$ ), then the rate at which the vertical field decreases must be moderated such that  $n=0.2$  occurs at the final ion radius.

Despite Robert R. Wilson’s rigorous 1938 study of an ion’s oscillatory response to the cyclotron’s fields, the motion has been coined “betatron motion” from Donald Kerst’s similar 1941 analysis of electron orbits in his “betatron” accelerator [9,10]. Weak focusing was the orbit stability workhorse for early cyclotrons, synchrotrons, betatrons and synchrocyclotrons and has recently enjoyed a revival with the advent of compact superconducting cyclotrons and synchrocyclotrons for medical applications [11]. To solidify these fundamental beam orbit concepts, our cyclotron students induce and measure betatron motion under differing conditions.

### 2.2. Axial Betatron Motion

Small axial motion is initiated by a vertical electric field that imparts an upward kick to the ions immediately upon their exit of the ion source. Figure 2a shows a Simion simulation of ions crossing a radial reference plane in our “good” poletips’ WF field, showing the vertical ribbon of beam oscillating about the median plane and coming to a focus near the DEE edge, where  $n=0.2$ . Figure 2b is the corresponding experimental observation in the Rutgers 12-Inch Cyclotron generated by slowly drawing the phosphor screen probe along the same radial reference plane. The increased frequency of the axial oscillation with radius is a display of the growing field index,  $n$ . Both 3a and 3b exquisitely demonstrate adiabatic damping, which always prompts a lecture on normalized emittance.

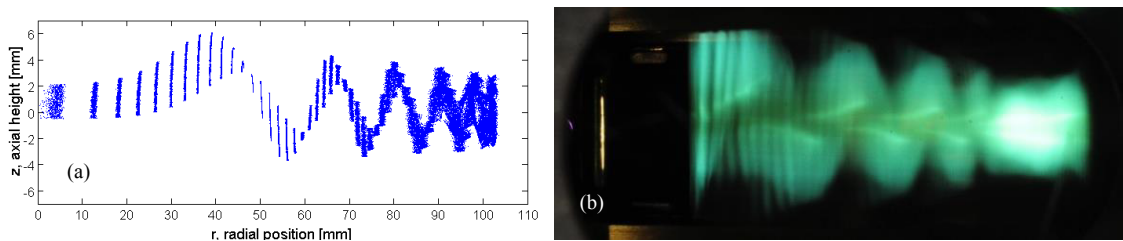


Fig. 2. (a) Simulated and (b) experimental observation of axial betatron motion in the Rutgers 12-Inch Cyclotron. Note large turn-to-turn separation in early revolutions at left of each image.

A typical cyclotron student exercise is to determine the tune, or equivalently, the field index as a function of radius [12]. One cannot directly measure the axial frequency; however, the beam phase advance per revolution can be measured with the phosphor plate drag image technique (figure 3b). From above, we can state that the axial betatron period of oscillation,  $T_z$ , relates to the ion revolution period,  $T_0$ :

$$T_z = \frac{1}{\sqrt{n}} T_0$$

Thus for a given  $n$  it takes  $1/n^{1/2}$  ion revolutions to complete one vertical betatron oscillation and it follows that the fraction which the betatron period advances at a given  $n$  per revolution is just  $n^{1/2}$ .

To estimate a local average tune,  $\nu_z$ , the student determines the radial locations of two adjacent axial peaks and divides by the number of revolutions within that interval. When the radial beam spot becomes wider than the turn-to-turn spacing, overlap prevents a direct count of individual turns; peak DEE voltage is used to estimate the number of turns within the corresponding energy (radial) increment. By definition, the measured tune directly follows from the ratio of vertical oscillations to revolutions. As an example, the reader can estimate from figure 2a - that  $\nu_z \approx 0.09$  at  $r=65$  mm.

### 2.3. Radial Betatron Motion

Initial ion radial-position errors can be introduced by horizontally sliding the chamber, and hence ion source, with respect to the magnet center. Since  $\nu_x(r=0)$  begins at 1, any radial offset simply displaces the equilibrium orbit by the same. As the ions gain energy and spiral towards larger radii,  $\nu_x(r)$  begins to drop, causing the location of

maximum radial displacement to azimuthally process. This continues until a tight inter-turn bunching occurs on one side of the cyclotron chamber while large turn to turn spacing develops on the other, as shown in figure 3. This feature has been exploited to increase extraction efficiency by placing the extraction septum at a location of amplified turn-to-turn spacing. Radial displacements can be translated to axial when  $v_x=2v_z$  ( $n=0.2$ ) is crossed and thus need to be avoided or transitioned rapidly.



Fig. 3. Demonstration of radial betatron motion leading to increased turn-to-turn spacing at large radii noted at image right.

#### 2.4. Destructive Resonance

We have built a set of poletips designed to intentionally drive a destructive axial resonance; we refer to these as the “bad” weak focusing poles tips. The  $n=0.2$  location occurs near  $r=3.5$  inches, well within the 5 inch DEE radius, so as to allow the ion displacement to grow. Since the  $n=0.2$  is a difference resonance the axial peak-to-peak amplitude is bounded by the initial radial offset. A displacement of the chamber’s center of about 3mm with respect to the magnet center was necessary to seed the resonant axial blow up to simulated and observed amplitudes of 6mm shown in figure 4.

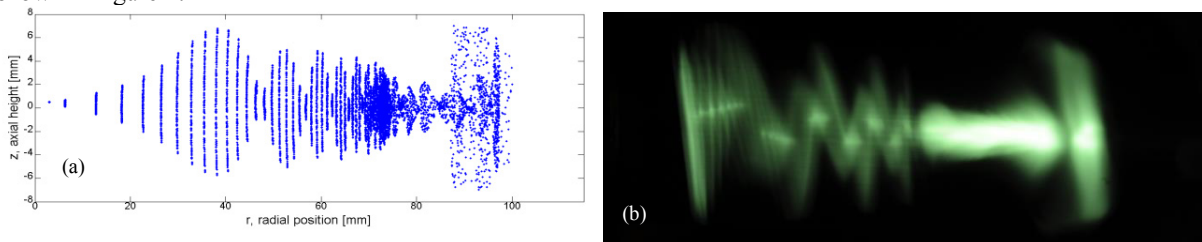


Fig. 4. (a) Simulated and (b) experimental observation of axial beam blow up at  $n=0.2$  resonance with “bad” WF poletips.

#### 2.5. AVF Focusing

The desired radial focusing field components of WF poletips imposes an undesirable decreasing vertical field dependence with radius in the median plane,  $B_z(r)$ , thus the cyclotron frequency varies along the beam’s spiraling path. Since the radio frequency power system typically operates at a single fixed frequency, there will be a mismatch between  $f_{cyc}$  and  $f_{rf}$  for most  $r$ . This mismatch is further exacerbated when the relativistic mass increase is encountered and places an upper limit on the energy attainable in the weak focusing cyclotron [13].

Thomas proposed a magnetic field configuration, which not only would provide comparable focusing, but would also accommodate relativistic effects [14]. In the Thomas field, the restoring force is generated by an azimuthally varying field (AVF) while the average vertical magnetic field is permitted to grow with radius so as to keep the relativistic mass increase  $f_{cyc}$  in sync, or isochronous, with the fixed frequency of the RF system.

In contrast to the WF axial restoring force, which we saw earlier develops from the ions’ angular velocity and radial magnetic field component, namely  $F_z=qv_\theta B_r$ , the vertical restoring force in radial sector AVF focusing arises from an ion’s radial velocity interacting with the magnetic field’s azimuthal component,  $F_z=qv_r B_\theta$  [15]. There are then two parameters contributing to the AVF axial restoring force:  $v_r$  and  $B_\theta$ . First, the ion’s radial velocity component,  $v_r$ , arises from the change in vertical field strength, and hence bending radius, between a high field (hill)



and low field (valley) regions. The rms variation of the vertical hill and valley magnetic field, called flutter and denoted as  $F$ , is the second contributing factor. The azimuthal magnetic field component,  $B_\theta$ , encountered at the transition of a hill and valley is proportional to the flutter.

In the AVF field, axial focusing can be further enhanced by instantaneously tilting the sector edge by an angle,  $\xi$ . Continuously applying an edge angle will result in a spiral sector edge from the center to the periphery. The tilting of the sector edge, projects a portion of the radial sector's  $B_\theta$  component into the radial direction:

$$B_r = -B_\theta \tan(\xi),$$

invoking another  $qv_\theta B_r$  force. Note that this  $B_r$  is separate from the weak focusing  $B_r$ .

For small to medium cyclotrons (1 to 10 MeV) AVF focusing can be used to supplement weak focusing. In this context, the weak focusing comes from the average radial gradient's field index, denoted as  $k$ , where:

$$k = \frac{d \ln \langle B \rangle}{d \ln R}.$$

The tune is proportional to the relative focusing strength. The axial tune in terms of the average field index, flutter ( $F$ ), and the instantaneous edge angle can be summarized by:  $\nu_z^2 = -k + F(1 + \tan^2 \xi)$  and the radial tune is written as:  $\nu_r^2 = 1 + k$

A balance is sought in the design of AVF pole to maximize  $\nu_z$  for the entire duration of the ions path, while avoiding destructive resonances associated with integer and rational fractional values of both  $\nu_z$ , and  $\nu_r$ .

To gain deeper illumination on the focusing properties of azimuthally varying fields, the Rutgers 12-Inch cyclotron group has constructed two sets of AVF poletips for experimentation [16]. The first set was a simple, pure-radial sector design of periodicity four. Their geometry was the least expensive to machine and provided the maximum field variation achievable within practical constraints. Not expected to host beam, their purpose was to benchmark simulations, measurement techniques, and test analysis code for the upcoming student AVF project.

The second set of AVF poletips are the product of an ambitious design program assigned to the Spring 2011 Cyclotron Students. Using the design tools developed with the pure radial sector poles, the students designed, constructed, measured and commissioned a set of pole tips that employed an Archimedes spiral, which successfully transported beam from the ion source to the periphery. Their pole tip set, shown installed in Figure 5a, was a four-sector Archimedean spiral sweeping 270 degrees, and will herein be referred to as AKG270. With the exception of the weak focusing central region, these pole tips aimed to satisfy the isochronous condition, in order to minimize the  $f_{\text{cyc}}/f_{\text{RF}}$  phase slippage, reduce the minimum required DEE voltage and preserve axial stability throughout the accelerating region.

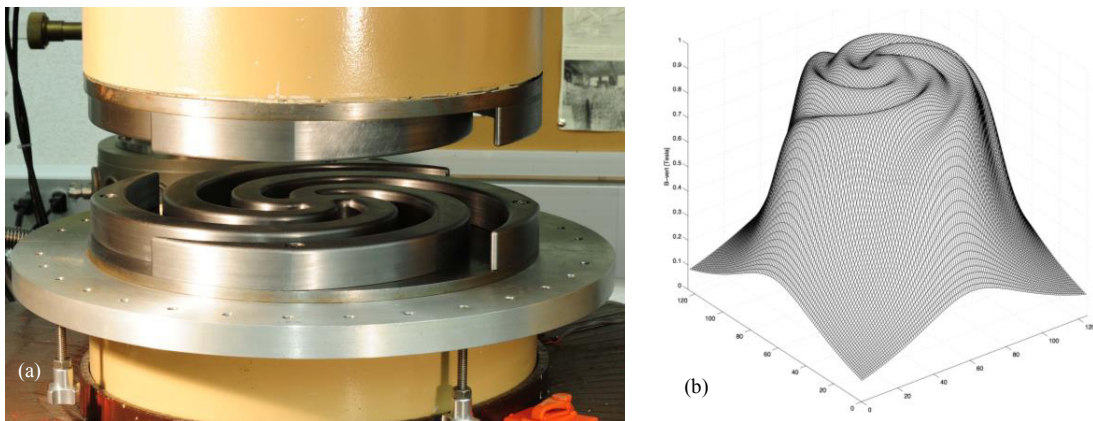


Fig. 5 (a) AKG270 spiral sector AVF poletips installed (b) 2-D  $B_z$  median plane field map measurement of poletips.

To verify the modeled magnetic field of the spiral AVF poletips, a 2-D field map of  $B_z$  in the median plane was performed. The measured magnetic field data plotted in figure 5b clearly displays the three features contributing to the focusing, first, the azimuthally symmetric weak focusing field drop off in the center which transitions into the AVF hill-valley flutter sectors which are spiraled. There is less than 1% variation between the measured and simulated region up to the maximum ion radius of 5-inches. The average vertical magnetic field radial profile quickly falls off from the central weak focusing contribution and is then followed by a constant isochronous field until the magnet's edge is neared.

During the design phase, Simion was used to determine the orbit characteristics of the various test-case magnetic fields. Protons, with a distribution of initial positions, were launched in the simulated magnetic fields with the accelerating RF off, performing so called “static simulations,” however the physical aperture of the DEE remained to define the limiting boundaries. The ions' subsequent motion was recorded to establish the limits of the stability in both the radial and axial extents. Radial and Axial phase space plots, such as shown in figure 6a, were generated and plotted in 50 keV increments up to the final design energy.

An interesting feature developed in the AKG270 radial trace space with energy. As early as 50 keV, the onset of non-linear motion was noted in the larger stable orbits. It exhibited four-sided contours, behavior which is consistent of AVF fields with a four-fold periodicity. The corners of the four-sided nonlinear orbits become more pronounced and bulbous with increasing energy. At 250 keV four closed contours formed in the protracted corners, displayed in Figure 6a. Thus, in addition to the primary equilibrium orbit, the simulations identified four off-center stable orbits.

The off-center equilibrium orbits were experimentally verified using the wire-loop orbit technique [17]. A 30 AWG wire loop, with a circumference of 71 mm, was energized with a current of 2.5 amps and placed in the magnet gap. Myriad other stable orbits made it difficult to perform this experiment in the median plane; instead a clear acrylic sheet was placed on the bottom pole tip to provide a flat surface on which the wire loop could lay. The energized wire loop simply needed to be tossed towards the gap and it would reproducibly snap to the nearest stable orbit. An overlay of multiple images displays five stable orbits shown in figure 6b. This technique found another four orbits (for a total of nine) located even further away from the center. Since the wire-loop technique does not discriminate based circumference (only the loop's tension will vary), the further outlying orbits are most likely lower energy equilibrium orbits.

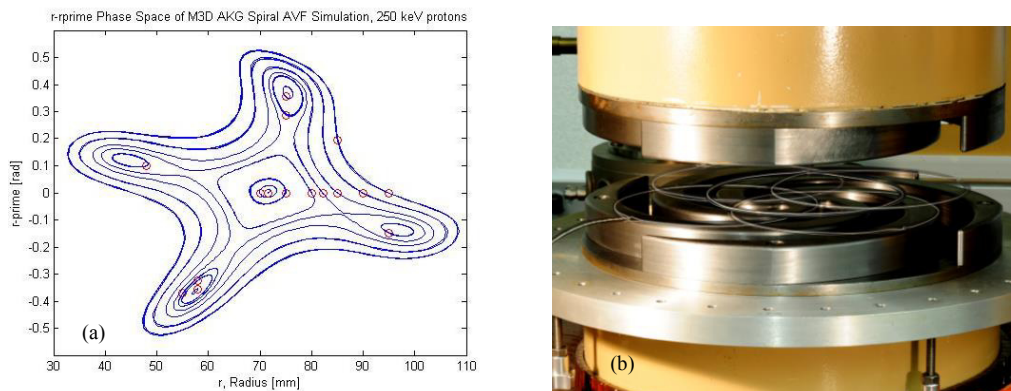


Fig. 6. (a) Radial phase space plot of 250 keV protons reveals five stable orbits; (b) Overlay image of a current carrying wire loop locating and demonstrating the five stable orbits.

The final test of the AKG270 pole tips was their operation with beam. The first radial draw image, shown in figure 7 shows a substantial increase in the axial betatron frequency compared to the WF pole tips, a result of the rapid drop off in the central field. The measured tune, in the flat AVF region  $\nu_z(r)$  is approximately 0.3.

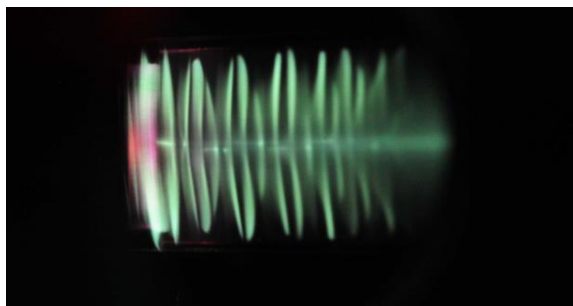


Fig. 7. First operation of the AKG270 spiral sector azimuthally varying field poletips displaying substantial increase in axial focusing.

## 2.6. Beam Energy Characterization

Large amplitude axial betatron motion has been characterized in our cyclotron and the axial phase advancement per revolution has been measured for several radii. Although, these image-based measurements agree with the implied beam energies for ions circulating at the given radii, it was deemed prudent to perform an absolute beam energy measurement at a single radial location. An assigned student project was the development and testing of a diagnostic to measure the absolute ion energy near the periphery.

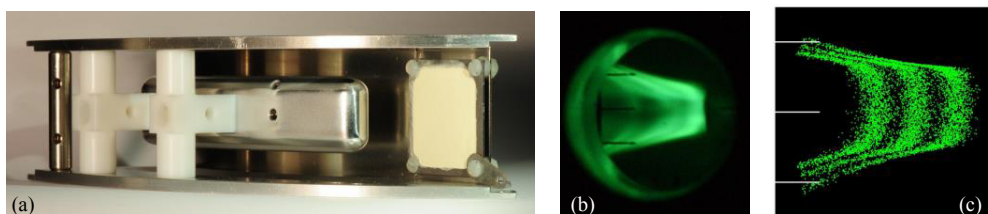


Fig. 8. Electrostatic deflection channel (a) modular hardware (b) in operation with beam on screen and (c) Simion simulation.

The cyclotron student produced a demountable electrostatic deflection channel, shown in figure 8a, that uses a transverse electric field to partially counter the magnetic field's orbit curving force. A thin, curved, grounded sheet, called the septum, forms a boundary between the main cyclotron accelerating volume and the deflection channel. A slightly greater curved high voltage (HV) electrode is concentrically arranged to form the ion deflection channel with an average 0.31 inch gap spacing. The deflector tangentially intercepts the spiraling cyclotron beam at a radius of 4.0 inches and transports the beam to a radius of 4.5 inches in  $43^\circ$  of azimuth. Since the deflection channel had a nominal radius of curvature of 7 inches, but intercepts the cyclotron beam at a radius of 4 inches, ions entering the de-energized channel will impinge on the septum and quickly be lost. A negative high voltage applied to the electrode generates a deflecting transverse electric field; only when an appropriate electric field is achieved will the magnetic field's bending force be partially negated permitting the transmission of ions to the phosphor screen. A greater electric field will cause the ions to terminate on the deflector and be lost, and a lesser field will cause the ions to terminate on the septum, only ions of the correct  $q/m$  ratio and velocity will be permitted to pass completely through the channel to be successfully detected. Thus the channel acts as a velocity filter, also known as a Wien Filter, enabling measurements of our ion beam's central energy and energy spread.

Beam transported to the end of the deflection channel is viewed on a phosphor screen that is mounted at a  $45^\circ$  angle with respect to the incident beam and to the axis of a vacuum view port, Fig. 8a. During operation several features are noticed: first, the upper and lower portions of the beam are horizontally distorted and secondly the imaged beam displays bands. A full 3D SIMION simulation of the deflector assembly has been performed to understand both. The 'smearing' is caused by the fringing electric field of the electrode's finite extent. The bands were determined to be compilations of multiple revolutions. Because the turn-to-turn spacing of the high-energy



circulating ion beam has become smaller than the radial width of a given turn-to-turn spacing, an iterative partial scraping of the final few turns occurs. Ions with sufficient radial extent in the  $n^{\text{th}}$  turn are captured by the channel and form the outer (right most) band in figure 8b. Those not intercepted continue on for another revolution,  $n^{\text{th}}+1$ , of acceleration, and thus have a greater rigidity and hence are deflected less forming the second band, and so it goes for the third band, or  $n^{\text{th}}+2$  turn. This was verified by simulation: 385, 405, and 425 keV ions were admitted to the deflector resulting in a comparable target image, figure 8c. Considering the finite width of the deflector entrance slit and channel, the resolution has been calculated to be 10% at 500 keV.

### 2.7. Beam Bunch Length

There is a tendency to envision the cyclotron beam as a continuous stream of ions from the source to the final target, while in fact the spiraling beam is comprised of minute bursts of ions captured during a limited period every RF cycle. Motivated to assist a Proton Beam Radiotherapy project, the three 2013 cyclotron students developed a technique to measure the proton bunch length in a single RF cycle [18]. A “fast” phosphor screen with a 3ns decay constant was viewed by a 3ns gated camera. The camera gating was triggered in sync with the Cyclotron RF and stepped through the RF cycle in 3 ns (or  $9^\circ$  of phase) increments. The resulting images could be stitched together to create a looped moving picture that depicts the pulsed nature of the cyclotron beam; the movie can be view on the Rutgers Cyclotron website. Frame-by-frame analysis, displayed in figure 9, revealed that ions nominally populate  $40^\circ$  of the  $360^\circ$  RF cycle in our cyclotron.

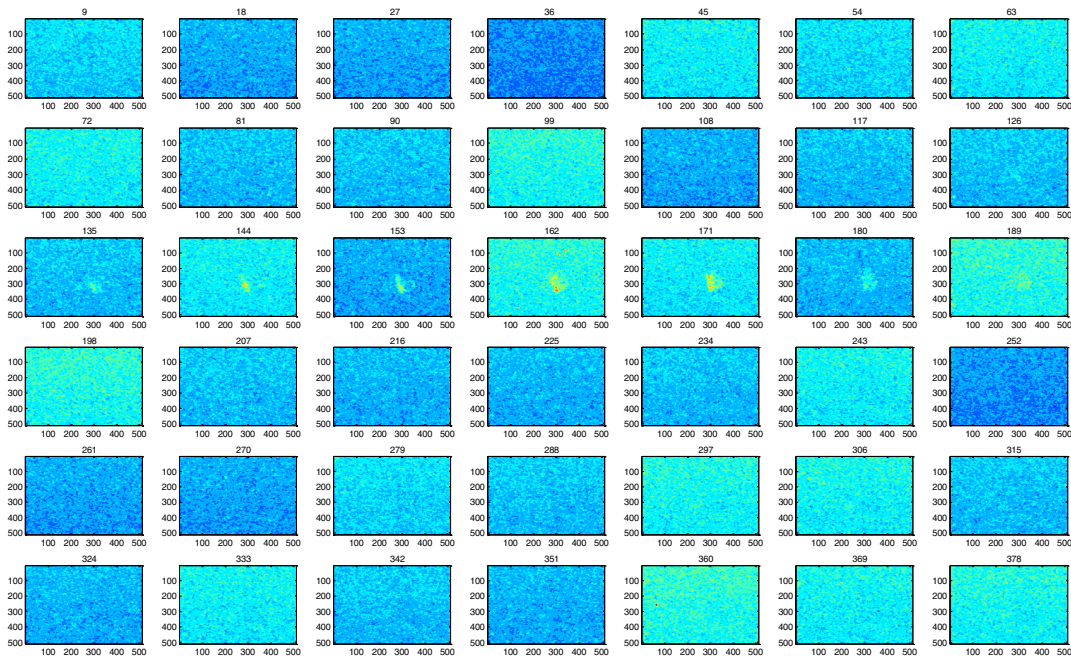


Fig. 9. Frame-by-frame analysis, in  $9^\circ$  increments, of proton beam on a phosphor target during a single  $360^\circ$  RF cycle.

### 3. Conclusions

The Rutgers 12-inch cyclotron in-lab accelerator has proved a successful didactic tool. Approximately one quarter of the twenty Modern Physics Lab cyclotron students have continued to pursue accelerator physics in both academia and industry. In addition to the standard spring semester students, our cyclotron program has hosted nearly

ten independent research studies in physics during the summer and spring sessions, and our machine has been incorporated into numerous Rutgers outreach programs, including QuarkNet and NJ AAPT.

Our cyclotron's educational impact extends beyond the Modern Physics Lab. Multiple institutions, such as Houghton College, Clemson University, IIT Madras, COLUMBUS CYCLOTRON and Jefferson Lab-Old Dominion, have acknowledged our cyclotron's educational impact by similarly developing their own teaching accelerators [19, 20, 21]. Several courses in the United States Department of Energy's Particle Accelerator School (USPAS) have utilized the many educational demonstrations of the Rutgers Cyclotron. The summer 2015 USPAS session, hosted by Rutgers, will offer a full semester equivalent cyclotron course taking advantage of daily labs with our accelerator.

## Acknowledgements

The author would like to acknowledge and thank the many individuals and institutions that have made our program a success. First the Rutgers Cyclotroneers, Stuart Hanebuth, Dan Hoffman, William Schneider, James Krutzler and Tim Ponter, whose generous volunteer efforts made this project a reality. A special thank you to Timothy Antaya for his guidance and ion sourcing, and to Robert Krawchuck for the donation of unobtainable equipment. Professor Kalelkar, the Rutgers Educational Physics Fund, the Rutgers machine shop, and the University of Maryland's Institute for Research in Electronics and Applied Physics for support through funds and equipment.

## References

- [1] Feder, T. "Building a Cyclotron on a Shoe String," Physics Today, 30-31, November 2004.
- [2] [www.physics.rutgers.edu/cyclotron](http://www.physics.rutgers.edu/cyclotron)
- [3] Koeth, T., "Report on the 12-Inch Cyclotron Magnet Study: Measurements, Modeling, and Future plans," [http://www.physics.rutgers.edu/cyclotron/papers/12\\_inch\\_magnet\\_studies\\_4.pdf](http://www.physics.rutgers.edu/cyclotron/papers/12_inch_magnet_studies_4.pdf), 2005
- [4] Koeth, T.W., Hine, G.A., Hoffman, D.E., Krutzler, J.E., Ponter, T.S., Rosenberg, A.J., Ruisard, K.J., Schneider, W.S., "Comparison of Azimuthally Varying with Constant Gradient Magnetic Fields with the Rutgers 12-Inch Cyclotron" [http://www.physics.rutgers.edu/cyclotron/papers/AVF\\_study\\_Dec\\_31\\_2011.pdf](http://www.physics.rutgers.edu/cyclotron/papers/AVF_study_Dec_31_2011.pdf), December 2011
- [5] Koeth, T.W., "Theoretical Calculations and Measurements of the DEE Voltage in the Rutgers 12 Inch Cyclotron" [http://www.physics.rutgers.edu/cyclotron/papers/12\\_inch\\_dee\\_voltage.pdf](http://www.physics.rutgers.edu/cyclotron/papers/12_inch_dee_voltage.pdf), December 2011
- [6] Koeth, T.W., Hoffman, D.E., Krutzler, J.E., Ponter, T.S., Rosenberg, A.J., Schneider, W.S., "Rutgers 12-Inch Cyclotron: Dedicated to Training through R&D," Proceedings WEPPT024 Cyclotrons 2013, Vancouver Canada, September 2013
- [7] Koeth, T.W., Hoffman, D.E., Krutzler, J.E., Ponter, T.S., Schneider, W.S., "Rutgers 12-Inch Cyclotron Electrostatic Deflector," [http://www.physics.rutgers.edu/cyclotron/papers/Deflector\\_Dec\\_31\\_2011.pdf](http://www.physics.rutgers.edu/cyclotron/papers/Deflector_Dec_31_2011.pdf), September 2010
- [8] [www.simion.com](http://www.simion.com)
- [9] Wilson, R.R., "Magnetic and Electrostatic Focusing in the Cyclotron," Phys. Rev. 53:408-420, 1938
- [10] Kerst, D.W., and Serber, R., "Electronic Orbits in the Induction Accelerator," Phys. Rev. 60:53-58, 1941
- [11] Antaya, T.A., "High-field Superconducting Synchro-cyclotron," Patent, PCT/US2007/001628, USA, 2007
- [12] Koeth, T.W., "Beam Physics Demonstrations with the Rutgers 12-Inch Cyclotron" WEPPT025 Proceedings of Cyclotrons 2013, Vancouver, BC, Canada, September 2013
- [13] Bethe, H., Rose, M.E., Phys. Rev. 52, 1254, 1937
- [14] Thomas, L.H., Phys. Rev. 54, 580, 1938
- [15] Livingood, J.J. "Principles of Cyclic Particle Accelerators," D. Van Nostrand, 1961
- [16] Ruisard, K.J., Hine, Koeth, T.W., Rosenberg, A.J., "The Rutgers Cyclotron: Placing Student's Careers on Target" WE1PB02 Proceedings of Cyclotrons 2013, Vancouver, BC, Canada, September 2013
- [17] Anderson, H.L., and Marshall, J., University of Chicago, Synchrocyclotron Progress Report, I, July 1947 – July 1948
- [18] Gonski, J.L., Burcher, S., Lazarov, S., Krutzler, J., Koeth, T.W., Beaudoin, B., "A Novel Optical Method for Measuring Beam Phase and Width in the Rutgers 12-Inch Cyclotron," WE1PB04 Proceedings Cyclotrons 2013, Vancouver BC Canada, September 2013
- [19] Yuly, M.E. "The Houghton College Cyclotron: a Tool for Educating Undergraduates" WE1PB01 Proceedings Cyclotrons 2013, Vancouver BC Canada, September 2013
- [20] Wolf, C.R., "COLUMBUS – A Small Cyclotron for School and Teaching Purposes," WE1PB03 Proceedings Cyclotrons 2013, Vancouver BC Canada, September 2013
- [21] Baumgartner, H., "The Cyclotron Kids' 2 MeV Proton Cyclotron" WE1PB05 Proceedings Cyclotrons 2013, Vancouver BC Canada, September 2013